ACS Sustainable Chemistry & Engineering

pubs.acs.org/journal/ascecg

Research Article

Impact of P3HT Regioregularity and Molecular Weight on the Efficiency and Stability of Perovskite Solar Cells

Narges Yaghoobi Nia, Matteo Bonomo, Mahmoud Zendehdel, Enrico Lamanna, Mohamed M. H. Desoky, Barbara Paci, Francesca Zurlo, Amanda Generosi, Claudia Barolo, Guido Viscardi, Pierluigi Quagliotto,* and Aldo Di Carlo*

Cite This: https://doi.org/10.1021/acssuschemeng.0c09015

Read Online

ACCESS | Metrics & More | Article Recommendations | Supporting Information

ABSTRACT: The commercialization of perovskite solar cells (PSCs) has seen an important limitation in the instability that afflicts the hole-transporting layer (HTL), namely, spiro-OMeTAD, used in high-efficiency devices. The latter is, in turn, relatively expensive, undermining the sustainability of the device. Its replacement with polymeric scaffolds, such as poly(3-hexylthiophene) (P3HT), will solve these issues. In this work, we adopted various sustainable synthetic methods to obtain four different homemade P3HTs with different molecular weights (MWs) and regioregularities (RRs), leading to different structural properties. They are implemented as HTLs in PSCs, and the effect of their properties on the efficiency and thermal stability of devices is thoroughly discussed. The highest efficiency is obtained with the highest MW and low-RR polymer (17.6%) owing to the more sustainable approach, but a very promising value is also reached with a lower-MW but fully regioregular polymer (15%). Finally, large-area devices with an efficiency of 16.7%, fabricated with a high-MW P3HT, show more than 1000 h (T80 = 1108 h) of stability under accelerated thermal stress tests (85 °C) out of glovebox while keeping over 85% of the initial efficiency of an unencapsulated device after more than 3000 min under continuous light soaking (AM 1.5G).

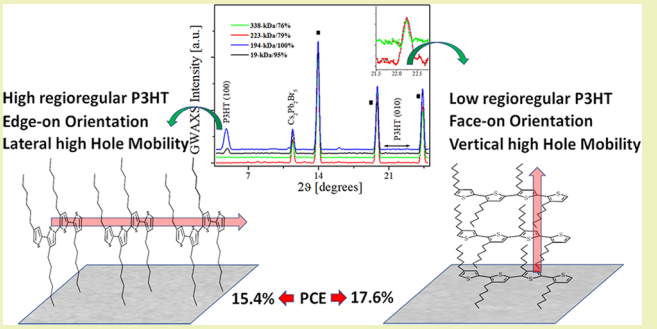

KEYWORDS: *P3HT, regioregularity, thermal stability, steric hindrance, molecular weight*

INTRODUCTION

The attention drawn by photovoltaic (PV) technologies based on hybrid organic−inorganic perovskite (PSK)-structured materials in these years is justified by the tremendous improvement in the power-conversion efficiency (PCE) that they have witnessed in less than a decade, going from just 3.8% up to 25.5%.[1−3] Such amazing PCE values in addition to the relatively low energy payback time (EPBT) and cost-effective solution-based production make perovskite solar cells (PSCs) a promising sustainable alternative for the near-future PV market.[4−6] However, one of the main limitations preventing perovskites from entering the PV market is the concern regarding their stability.[7−10] To comply with IEC standard 61215, thin-film PV devices should pass, among others, a damp heat stability test at 85 °C with 85% relative humidity (RH) for 1000 h. For this reason, several research groups are trying to address the stability issue for this technology, and "stable" has become a notorious word in the title of most publications on this topic.[11−14] The versatility of perovskites lies in their chemical composition, which can be tuned to satisfy specific requirements, e.g., band-gap tuning through halide substitution[15] or improved thermal and chemical stability by replacing the volatile methylammonium (MA) cation with formamidinium (FA) and cesium (Cs).[16,17] Another approach to tune the features of the absorbing layer deals with the exploitation of perovskite quantum dots (Pe-QDs).[18] Nevertheless, the thermal instability of perovskite solar cells (PSCs) is not only due to the perovskite (PSK) but also related to other layers in the device structure, in particular, charge-selective materials. Specifically, the n-i-p structure, which is currently the most efficient one reported in the literature,[19,20] employed 2,2′,7,7′-tetrakis-(*N*,*N*-di-4-methoxyphenylamino)-9,9′-spirobifluorene (known as spiro-OMeTAD) as HTM.[21] Spiro-OMeTAD, a small-molecule organic p-type semiconductor, was found to be the main cause of the thermal instability of perovskite-based devices because of its low glass-transition temperature and the volatility of the *tert*-butylpiridine (TBP) dopant, which is used to increase the hole conductivity.[22−25] The spiro-OMeTAD

Received: December 11, 2020
Revised: March 11, 2021

with additives undergoes crystallization at 85 °C and its hole mobility significantly deteriorates, hence causing thermal instability.[21] Generally, doping of the molecular-based HTMs (e.g., spiro-OMeTAD) can negatively affect the overall stability due to an increase in the natural hydrophilic effect of these HTMs and chemical degradation,[26] while in the polymeric HTM with long hydrophobic chains, selection/optimization of the best doping mixture not only can improve charge extraction and overall efficiency of the device but also shows a promising stability toward humid air, thermal, and light stresses.[27−29] Such an improvement can be attributed to localization of the polaron induced by the dopant's mixture into the polymer chains (with a higher influence for longer polymeric chains).[30] Bonomo et al. employed thermosetting polyurethanes as encapsulant materials, proving a strong interaction with the hole-transporting layer (HTL) that results in an improved light and thermal stability.[31]

Aiming at replacing spiro-OMeTAD, different polymers are being investigated for application in PSCs, also because of the possibility to adjust their properties by acting on their molecular weight (MW).[32−37] Among these, a suitable candidate is poly(3-hexylthiophene) (P3HT), a material that has seen vast application in the field of organic photovoltaics (OPVs) as a donor polymer in bulk-heterojunction solar cells,[38] thermoelectric applications,[39] and organic light-emitting devices (OLEDs). P3HT has attracted great interest as a polymeric hole-selective material for PSCs due to its scalable solution processability,[40] high thermal stability,[41] low cost,[42] relatively high hole mobility (0.1 $cm^2\ V^{-1}\ s^{-1}$),[43] oxygen impermeability, wide band-gap,[44] and robust hydrophobicity.[45]

Recently, Jung et al. have demonstrated a 22.7% efficient PSC with P3HT as the HTL by passivating the perovskite/P3HT interface through the application of a wide band-gap halide (WBH) material to reduce undesired nonradiative recombination phenomena, which reduces the device's output voltage.[46] With this strategy, they also observed a good stability of over 1300 h under constant 1 sun illumination. In our previous works, we have also successfully used high-regioregular (RR around 96%) P3HT as the HTL and evaluated the influence of its molecular weight (MW) and mesoporous scaffold thickness on the performance of PSCs.[47] The results showed that increasing the MW of the polymeric hole-transporting material (HTL) enhances the PCE from below 5% for the lowest MW 44 kDa to over 16% for a 124 kDa P3HT transport layer.[47] Afterward, we also reported a perovskite PV module with P3HT exhibiting an efficiency of 13.3% on a large-area-module (43 cm^2) active area.[27] Nia et al. presented how the differences in MW and the differences in energetic disorder influence the interfacial carrier losses in the PSCs under operating conditions.[48]

Thermal stability is an important parameter for the commercialization of PV technologies; therefore, the materials that are used should not degrade under operating conditions even in the harshest environments. In organic polymeric semiconductors, the temperature increase enhances the chain motion, which could induce morphological degradation of the layer and consequently a reduced long-term stability of the device.[49] Many research groups have addressed this issue through the cross-linking approach, which can improve the thermal stability by reducing chain dynamics.[50−52]

Actually, when dealing with polymers, MW and RR are parameters that should be considered. The influence of MW of conjugated polymers on their stability and on their electrical and physical properties has been the subject of numerous studies in many different fields. In the PV field, a recent study by Kang et al. evidenced how the MW of the donor polymer in the PPDT2FBT:P(NDI2OD-T2) donor−acceptor blend could affect the performance of the obtained polymeric bulk-heterojunction solar cells.[53] In particular, they observed that higher MWs favored the "face-on" orientation of PPDT2FBT, which is the most favorable for improving hole transport among the chains, producing a 5-fold increase in hole mobility with respect to the lowest MW considered in the examination. Higher donor MW also favored the intermixing with the acceptor, thus positively influencing the electron mobility too.

Stability-wise, Wang and Hsieh correlated the thermal stabilities of two series of segmented poly(urethaneureas) thermoplastics with the molecular weight and structure of their soft segment.[54] Thermogravimetric analysis (TGA) carried out in both air and nitrogen and differential scanning calorimetry (DSC) revealed that a higher MW of the polyol soft segment corresponds to an improved thermal stability of TPUs, resulting in higher temperatures required to cause the same mass loss. Yang and co-workers studied the effect of poly(ethylene glycol) (PEG) MW on the thermal stability and dissolution behavior of a Griseofulvin PEG crystalline inclusion complex. They observed that thermal stability is improved with increasing MW, until reaching a plateau.[55] This is justified by the growth structure of the lamellae of the PEG polymer, which thickens as the MW increases up to 4 kDa, thus increasing the melting point of the material. For MWs higher than 4 kDa, the lamellae thickness does not change much because of a folded chain crystal growth, so no further change is observed in the thermal stability.[56,57] Huang et al. investigated the effect of RR of P3HT in the blend phenyl-C_{61}-butyric acid methyl ester (PCBM)−P3HT: by increasing the RR of the polymer, the thermal stability improved.[58] Kim et al. also showed that by enhancing the RR the photovoltaic efficiency of the device enhanced, and the influence of the RR on the improvement of the solar cell performance could be related to the enhanced optical absorption and transport resulting from the organization of the P3HT chain and domain,[59] while Sivula and co-workers showed that on increasing the RR, the stability decreased.[60] Chuang et al. reported that the RR effect on optical anisotropy increased the power-conversion efficiency of large-area P3HT/PCBM-based organic solar cells.[61]

In this work, we investigate the thermal behavior of four homemade P3HTs with different combinations of MWs/RRs, namely, 19 kDa/95%, 194 kDa/100%, 223 kDa/79%, and 338 kDa/76%, and their influence on the thermal stability of mixed-cation ($(FAPbI_3)_{0.81}(MAPbBr_3)_{0.14}(CsI)_{0.05}$) perovskite solar cells (small-area and large-area cells, Figure S2). Importantly, P3HT films of different RRs and MWs were investigated by means of X-ray diffraction (XRDs) measurements and grazing incidence wide-angle X-ray scattering (GIWAXS) analysis, and the role of the structural properties is discussed.

EXPERIMENTAL SECTION

All materials and methods, experimental data and procedures, polymer syntheses and characterizations, device preparation, tests, and characterizations are reported in the Supporting Information section.

https://doi.org/10.1021/acssuschemeng.0c09015
ACS Sustainable Chem. Eng. XXXX, XXX, XXX−XXX

RESULTS AND DISCUSSION

Synthesis and Characterization of P3HT Polymers. *Synthetic Procedures and Regioregularity.* Different synthetic methods were used to prepare the polymers.[62] A low-MW (19 kDa/95%) P3HT was prepared by the direct arylation protocol (DArP) method (Scheme 1, path a), showing a 95% RR,[62] while the GRIM (Grignard methathesis) method gave a very-high-MW P3HT (194 kDa/100%) with full RR (Scheme 1, path b).[62,63]

Scheme 1. Synthesis of P3HT with Different Structural Characteristics. Reactions Conditions: (a) K_2CO_3, $Pd(OAc)_2$, Neodecanoic Acid, Dimethylacetamide (DMA), 95 °C, 72 h; (b) (1) *i*PrMgCl, Tetrahydrofuran (THF), Room Temperature (rt), 1 h; (2) $Ni(IPr)(Acac)_2$, THF, 30 min; (c) $FeCl_3$, $CHCl_3$, rt, 24 h; (d) $FeCl_3$, $CoCl_2$ (10%), $CHCl_3$, rt, 24 h

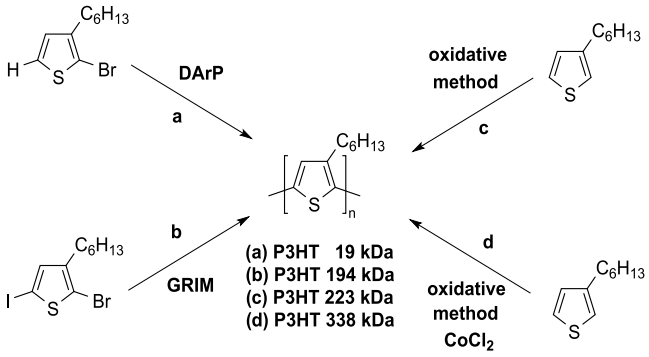

Finally, two high-MW P3HT polymers were obtained by an oxidative polymerization, induced by $FeCl_3$ as the oxidizing agent (Scheme 1, path c).[64] Since $FeCl_3$ can also induce, at least in part, a radical mechanism for polymerization, one of the polymers was obtained by adding also $CoCl_2$ (10% with respect to the monomer), which was known to act as a radical scavenger, thus suppressing the radical polymerization pathway (Scheme 1, path d).[65] This was reported to help increase the molecular weight. However, the $FeCl_3$ method is known to produce polymers with low RR (70−80%).

For all of the soluble polymers (19 kDa/95%, 223 kDa/79%, 338 kDa/76%), the molecular weights were measured by size-exclusion chromatography (SEC), using THF as a solvent and working at 35 °C (for experimental details, please see the Supporting Information). ^{1}H-NMR spectra of the synthesized polymers have been presented in Figure S1.

The 194 kDa/100% polymer was insoluble in THF, and only less than 10% could be eluted during SEC. Due to this limitation, the SEC conditions were modified, using *o*-dichlorobenzene as the eluent, working at a very high temperature (145 °C).[66] In these conditions, the molecular weight could be easily determined. The results are reported in Table 1. The polymers with higher RR showed lower polydispersity (PDI), while the P3HT obtained by the oxidative method showed a higher PDI.

TGA and DSC of P3HT Polymers. The polymers were analyzed by thermogravimetric analysis (TGA) under N_2 to assess their thermal stability (Figure 1a). The decomposition temperature was in the range 425−441 °C, establishing the excellent stability of the polymers and their attitude to be processed for solar cells. The TGA plot of different MW P3HT is presented in Figures 1a and S3.

The differential scanning calorimetry (DSC) characterization (Figures 1b and S4) was performed under N_2, to assess the thermal behavior of the polymers, establishing the degree of crystallization and the dependence of the polymer behavior on the PDI. In general, higher crystallinity and lower PDI result in sharper high fusion peaks. The DSC thermal analysis showed a wide peak in the warming cycle for P3HT 223 kDa/79% and P3HT 338 kDa/76% at around 180−187 °C, which was attributed to the fusion of the crystalline domains of the polymers. This is consistent with the limited RR, around 76−79%, of these polymers, which are characterized by a predominance of amorphous regions as proved by the relatively low peak intensity. The recrystallization peak was found to occur at lower temperatures, around 89−102 °C (Table 2).

The P3HT 19 kDa/95% polymer showed a quite wide peak in DSC, attributed to the melting of crystallites. The crystallinity is quite high, but the wide peak suggests a somewhat large PDI for this short-MW P3HT or some content of irregularity. However, the 194 kDa/100% polymer showed a high and well-defined fusion peak (at a very high temperature, 235.5 °C), denoting the larger occurrence of crystalline regions. This is consistent with the full RR of this polymer. The crystallization peak occurs at 189.7 °C in the cooling cycle. The high RR, the limited PDI, and the high MW contribute to the high crystallinity, which in principle should be important to give good conductivity and hole mobility.[67−69]

UV Spectra of P3HT Polymers. The absorption (solid line) and emission (dashed line) UV spectra are reported in Figure 1c. It is well-known that high RR hampers the solubility of P3HT in many solvents due to the close packing allowed by the alkyl chain interaction between different polymer chains, even at relatively high temperatures.[62]

After a first trial to perform the UV measurements in dichloromethane and/or chloroform, we had to resort to dichlorobenzene as the solvent. Notwithstanding, the fully regioregular polymer (194 kDa/100%) showed the appearance of a small peak around 610 nm, which indicates the presence of a minimal quantity of aggregates even in solution. The UV

Table 1. Structural Characterization of P3HT Polymers (for the Synthetic Methods, See the Text)

P3HT polymer	338 kDa/76%	223 kDa/79%	194 kDa/100%	19 kDa/95%
method	oxidative ($CoCl_2$)	oxidative	GRIM	DArP
yield [%]	41.4	42.7	81.8	91.0
RR[a]	76	79	100	95
M_n [kDa]	61[b]	55[b]	69[c]	8.2[b]
M_w [kDa]	338[b]	223[b]	194[c]	19[b]
PDI	5.6[b]	4.1[b]	2.8[c]	2.3[b]

[a]Regioregularity. [b]MW determined by SEC in THF at 35 °C. [c]MW determined by SEC in *o*-dichlorobenzene at 145 °C.

https://doi.org/10.1021/acssuschemeng.0c09015
ACS Sustainable Chem. Eng. XXXX, XXX, XXX−XXX

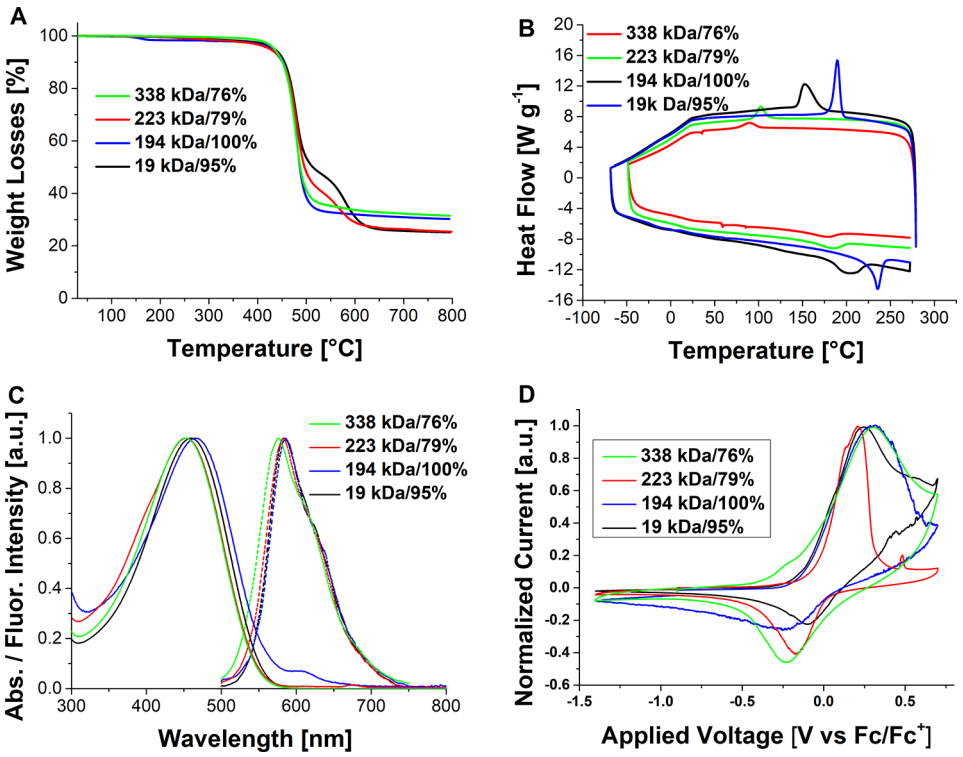

Figure 1. TGA (A) and DSC (B) curves, absorption (solid line) and emission (dashed line) spectra (C), and cyclovoltammetric measurements (D) of 19 kDa/95% (black), 194 kDa/100% (blue), 223 kDa/76% (red), and 338 kDa/76% (green).

Table 2. Thermal, Optical, and Electrochemical Properties of Synthetized P3HT Polymers

P3HT polymer	HOMO[a] (eV)	band gap[b] (eV)	LUMO[b] (eV)	λ_{max} (nm)	λ_{em} (nm)	heat. cycle[c] fusion (°C)	cool. cycle[c] cryst. (°C)	stability[d] (@95%) in N_2 (°C)
338 kDa/76%	−5.14	2.34	−2.80	453	575	180.3	89.1	434.5
223 kDa/79%	−5.10	2.32	−2.78	458	583	186.8	102.7	426.2
194 kDa/100%	−5.12	2.27	−2.85	467	586	235.5	189.7	441.3
19 kDa/95%	−5.13	2.29	−2.84	462	585	205.3	152.6	435.2

[a]From cyclic voltammetry. [b]From optical measurements. [c]From DSC. [d]From TGA.

maximum wavelength increases with the RR since the latter induces a higher conjugation length in the P3HT.[62] The choice of dichlorobenzene as the solvent was however beneficial, and the same solvent was used for the CV measurements (Figure 1d).

Electrochemical Characteristics of the Polymers and Their Thin Films. The electrochemical characterization of different MWs of P3HT showed similar features, with the highest occupied molecular orbital (HOMO) level of the four polymers being located at about −5.10 eV vs the vacuum, in accordance with literature reports.

The optical band gap was calculated from the intersection between the absorption and the emission spectra, and it was found to be close to 2.30 eV. The energy of the lowest unoccupied molecular orbital (LUMO) could be roughly estimated by the sum between the HOMO energy and the optical band gap, and it is close to 2.28 and 2.33 eV for regioregular and not-regioregular polymers, respectively.

It is worth mentioning that the electrochemical analyses were conducted on solubilized HTMs (in dichlorobenzene), but just slight changes are expected in the solid state. The optoelectronic properties of the HTMs seem to be uninfluenced by the different synthetic approaches and, in turn, by the different molecular weights or RRs of the polymers. Therefore, we are quite confident that any difference in the photoelectrochemical behavior of the corresponding PSCs could be ascribed to morphological, interfacial, or stability issues.

Electrochemical impedance spectroscopy (EIS) is a very sensitive detector of interfacial modification. Potentiostatic EIS of different MWs of P3HT (fluorine-doped tin oxide, FTO/P3HT/Au, Schottky diode structure) has been evaluated under dark conditions and zero bias voltage. Nyquist plots are composed of one semicircle at low frequency (the equivalent circuit is reported as an inset) (Figure S5), R_s is mainly related to the resistance of the FTO substrate.[70,71] The semicircle in the low-frequency range is associated with the recombination resistance (R_1) at the HTL/electrode interface.[47,72,73] The fitted values of the circuit elements are presented in Table S1. The results show a clear effect of MW tuning for blocking the interfacial recombination through marked enhancement of recombination resistance with MW increment of the P3HT.

On the other hand, to measure the carrier mobility of P3HT thin-film layers, dark JV curves of the Schottky diode of three polymers were measured, and the space charge limited current (SCLC) and carrier mobility (μ) parameters were extracted by fitting the dark JV curves in the SCLC equation and the Mott−Gurney equation,[74] and the results are listed in Table S2. The

https://doi.org/10.1021/acssuschemeng.0c09015
ACS Sustainable Chem. Eng. XXXX, XXX, XXX−XXX

results show similar magnitude changes of the carrier mobility of doped P3HT following an increase of the MW from 223 to 338 kDa. Such a molecular weight dependence of carrier mobility and recombination rate has been studied in neat undoped P3HT films.[75]

XRD and GIWAXS of Polymeric Thin Films. Preliminary XRD measurements were performed in the Bragg–Brentano configuration to evaluate the perovskite-layer crystalline structure of $(FAPbI_3)_{0.81}(MAPbBr_3)_{0.14}(CsI)_{0.05}$. As shown in Figure 2a, the presence of the substrate signal is also detected,

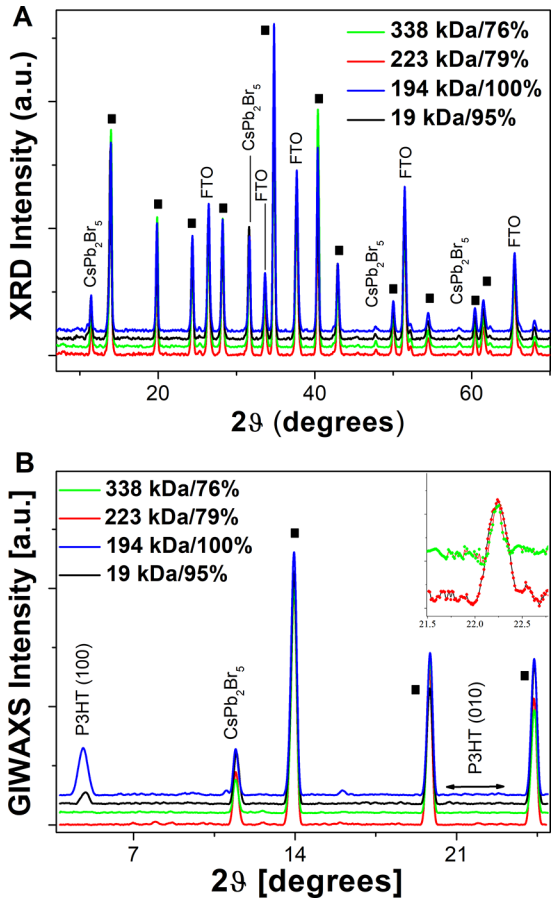

Figure 2. (A) XRD patterns of glass/FTO/perovskite/P3HT samples. Black squares are used to label perovskite reflections, and cesium lead bromide and FTO reflections are also indicated. (B) GIWAXS patterns of glass/FTO/perovskite/P3HT samples. Black squares are used to label perovskite reflections, and the cesium lead bromide reflection is also indicated. In the inset, the P3HT (010)-reflections observed from P3HT 223 kDa/79% and 338 kDa/76% samples are highlighted.

as expected, in all samples: FTO diffraction peaks are attributed accordingly to crystallographic ICDD Card Nr: 00-003-1114. Perovskite reflections are labeled with a black square, and Miller indexes are reported in Table S3.[76,77] A minor contribution of the cesium lead bromide $CsPb_2Br_5$ is also detected, with the (002) reflection at $2\theta = 11.6°$ and the (300) reflection at $2\theta = 31.60°$ being observed (according to ICDD card Nr: 00-025-0211). XRD patterns of all samples are perfectly overlapping regarding this preliminary investigation. Appearance of the Br-rich $CsPb_2Br_5$ diffraction signal in addition to the $(Cs,FA,MA)Pb(I,Br)_3$ perovskite phase could be attributed to the influence of the doped polymeric HTM on the perovskite/HTM interface. Such an interesting phenomenon has been observed on the perovskite/PTAA interface with a positive impact on device stability.[30,37]

Subsequently, samples were characterized by means of the GIWAXS technique to evaluate the P3HT layers' structural characteristics and detect possible modifications induced by different MWs and RRs. Observing the patterns in Figure 1b, a first comment can be made: samples P3HT 223 kDa/79% and P3HT 338 kDa/76% show a much lower crystalline contribution (inset of the figure) in comparison to samples P3HT 19 kDa/95% and P3HT 194 kDa/100%, films that are, in turn, the ones showing a higher RR.

Despite the GIWAXS measurements being performed "ex situ" upon different samples, using the substrate as an internal reference, it is possible with good confidence to affirm that the crystallinity (Bragg reflection intensity) of the high-MW films is considerably lower (≈1 order of magnitude) than the one observed upon the lower-molecular-weight samples, having a higher RR. Such evidence is, in turn, in good agreement with the DSC results reported above.

Analyzing the GIWAXS results in greater details, two different orientations of the crystalline P3HT domains with respect to the glass/FTO substrate are identified: the (100) reflections due to the lamella-layer structure and the (010) reflections due to $\pi-\pi$ interchain stacking. It is found that samples with higher RRs (19 kDa/95% and 194 kDa/100%) showed preferential orientation along the (100)-axis, normal to the film (edge-on configuration), with the polymers oriented with the alkyl chains stacked normal to the substrate.[78] The (100) reflection is observed at $2\vartheta = 4.82°$, corresponding to a distance d of 18.15 Å. On the contrary, samples with the highest MW and lowest RR are found to be oriented in a face-on configuration along the (010)-axis ($2\vartheta = 22.24°$), with the thiophene rings parallel to the substrate and a planar interdistance corresponding to d = 3.99 Å. The reflections corresponding to such a configuration are evidenced in the inset of Figure 2b.[79−82]

Perovskite Solar Cells. *Photovoltaic and Optical Performances of Small- and Large-Area PSCs.* Photovoltaic parameters of small-area PSCs using different synthesized P3HTs as HTL were measured under 1 sun AM 1.5G illumination, and the statistic box plots of their PCEs are shown in Figure 3a. Other PSC (PCE vs MW and RR) parameters are presented in Figures S6 and S7. In particular, a trend emerges from Figure 3a, suggesting that the PCE of the PV devices is directly related to the increase in MW of the P3HT, confirming our previous findings.[33] Devices fabricated with the 19 kDa polymer are the worst-performing ones, exhibiting the lowest V_{oc}, fill-factor (FF), and J_{sc}. Furthermore, these devices also show the highest statistical dispersion related to worse reproducibility. The best efficiency was obtained for the highest MW P3HT polymer (338 kDa), reaching a PCE of 17.6% for a small-area device (active area 0.1 cm^2). The increment compared to intermediate MWs (194 kDa/100% and 223 kDa/79%) comes from the slightly enhanced J_{sc} and V_{oc} and mainly from the FF increase, as shown in Figure S6. J_{sc} increased considerably from low to high MW; increasing the J_{sc} also could be related to the higher RR,[51] as shown in Figure S7.

The comparison between P3HT with similar RR permits one to directly assess the impact of the MW on the PCE. By increasing the MW from 19 to 194 kDa (both with RR around 95−100%), the average PCE increases from 9 to 13% (+44%).

https://doi.org/10.1021/acssuschemeng.0c09015
ACS Sustainable Chem. Eng. XXXX, XXX, XXX−XXX

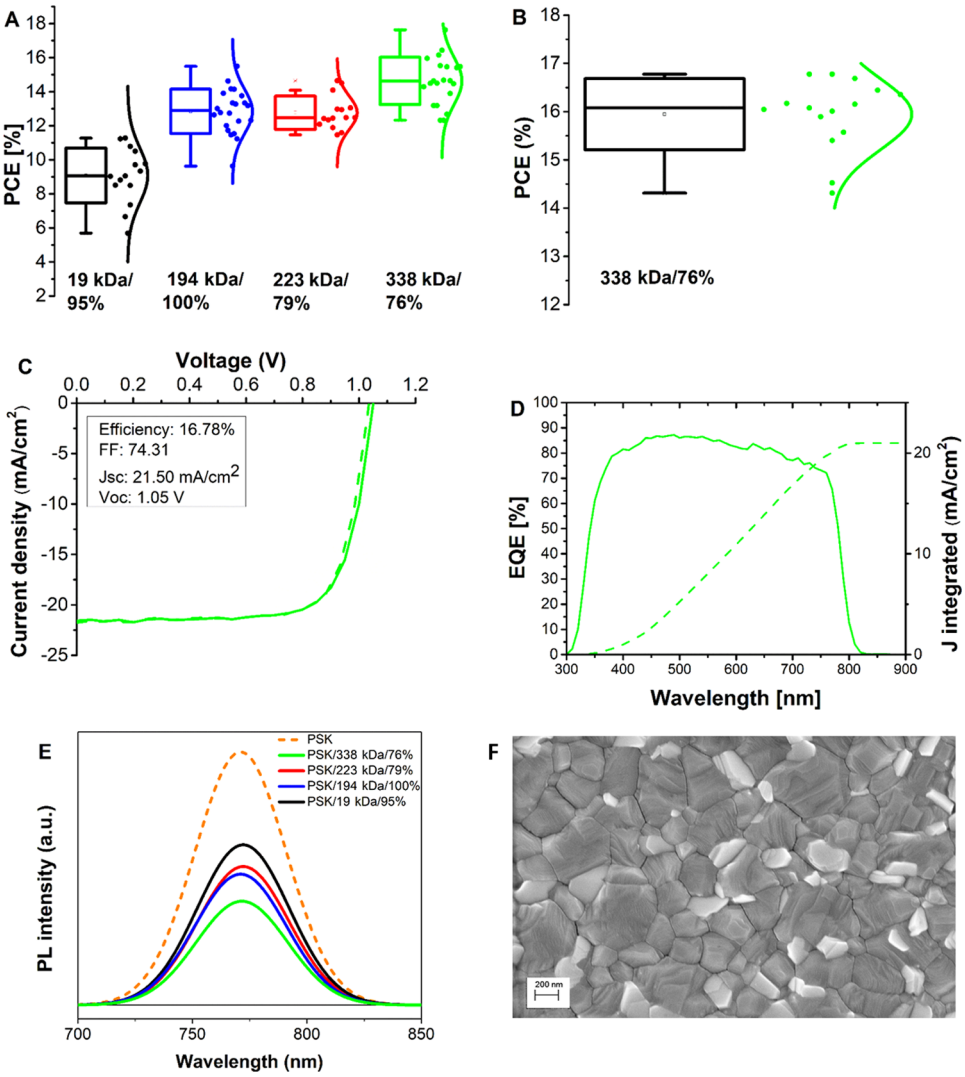

Figure 3. (A) PCE for small-area cells with different MWs. (B) PCE for high-MW large-area cells. (C) IV of the champion high-MW large-area device; the reverse scan from V_{oc} to 0 and the forward scan from 0 to V_{oc} are represented by solid and dashed lines, respectively. (D) Incident photon-to-current conversion efficiency (IPCE) of the champion device. (E) Photoluminescence (PL) curves of the perovskite-based layers with different MWs of P3HT. (F) SEM images of the bare PSK layer.

Similarly, by increasing the MW from 223 to 338 kDa (both with RR around 76−79%), the average PCE increases from 12.4 to 14.7% (+20%). We should however notice that, while the MW increment is sufficiently similar for the two cases (+110 vs +175 kDa), the increment of the efficiency is just half. At the same time, we can assess the impact of RR on the performance of the cells by comparing the two average MW P3THs, which have quite different RRs. The performances of PSCs with 194 kDa/100% (average PCE = 13%) clearly outperformed the ones of PSCs with 223 kDa/79% (average PCE = 12.4%): indeed, for the PCEs, the slightly lower MW of the 194 kDa/100% one with respect to the 223 kDa/79% (−27 kDa) one is positively counterbalanced by a notably higher RR (+21%). This leads us to the conclusion that to obtain high-performing PSCs, embodying P3HT as the HTL, the latter should present a higher MW and RR as much as possible.

The reported results would hint at the fact that shorter polymer chains hinder charge extraction from the perovskite active layer, therefore reducing the FF; this also results in a higher nonradiative recombination rate at the interface, which jeopardizes the V_{oc} of the device.[69,70] On the other hand, the improvement in J_{sc} could be related to the better hole mobility of high-MW P3HT compared to the low-MW one. Higher FF could be related to the increase in conductivity of the higher MW (doped) with respect to the lowest MW (doped) and could be due to the better interface contact between the perovskite and HTL and also between HTL and gold.[47]

Furthermore, to evaluate the scalability of the best polymeric HTL, a batch of large-area devices using 338 kDa/76% P3HT as the HTL has been fabricated and the statistic box plots of their (PCE) parameter are presented in Figure 3b, while their FF, V_{oc}, and J_{sc} are presented in Figure S8. The champion large-area device has a PCE of 16.7%, V_{oc} of 1.05 V, J_{sc} of 21.5 mA/cm^2, and FF of 74% with almost no hysteresis, as shown in Figure 3c. Incident photon-to-current conversion efficiency (IPCE) measurement confirms the J_{sc} extracted from the IV measurements (Figure 3d).

Photoluminescence (PL) curves of the perovskite-based layers are presented in Figure 3e. The PL emission peak at 772 nm is quenched significantly in the sample with PSK/P3HT with respect to the bare perovskite layer. The reduced PL

https://doi.org/10.1021/acssuschemeng.0c09015
ACS Sustainable Chem. Eng. XXXX, XXX, XXX−XXX

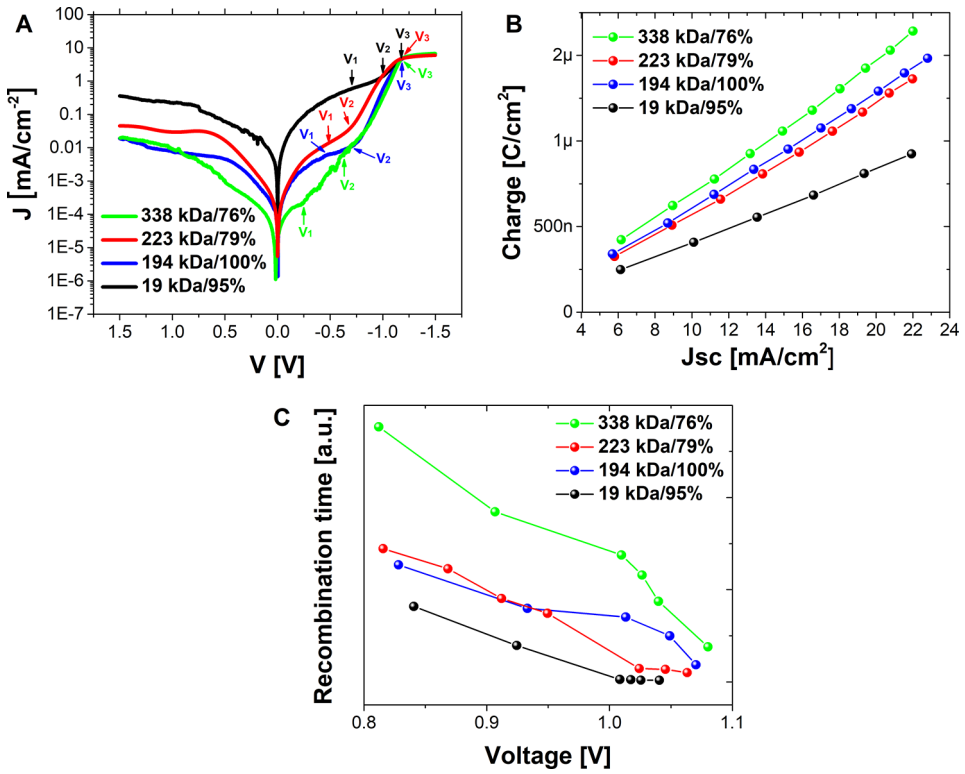

Figure 4. (A) Tafel plots of the PSCs with different MWs of P3HT as HTL evaluated from cyclic voltammetry analysis. (B) Charge extraction curves of the PSCs obtained from transient photocurrent (TPC) fall/rise analysis. (C) Recombination time versus voltage, evaluated from the transient photovoltage (TPV) decay analysis of the PSCs.

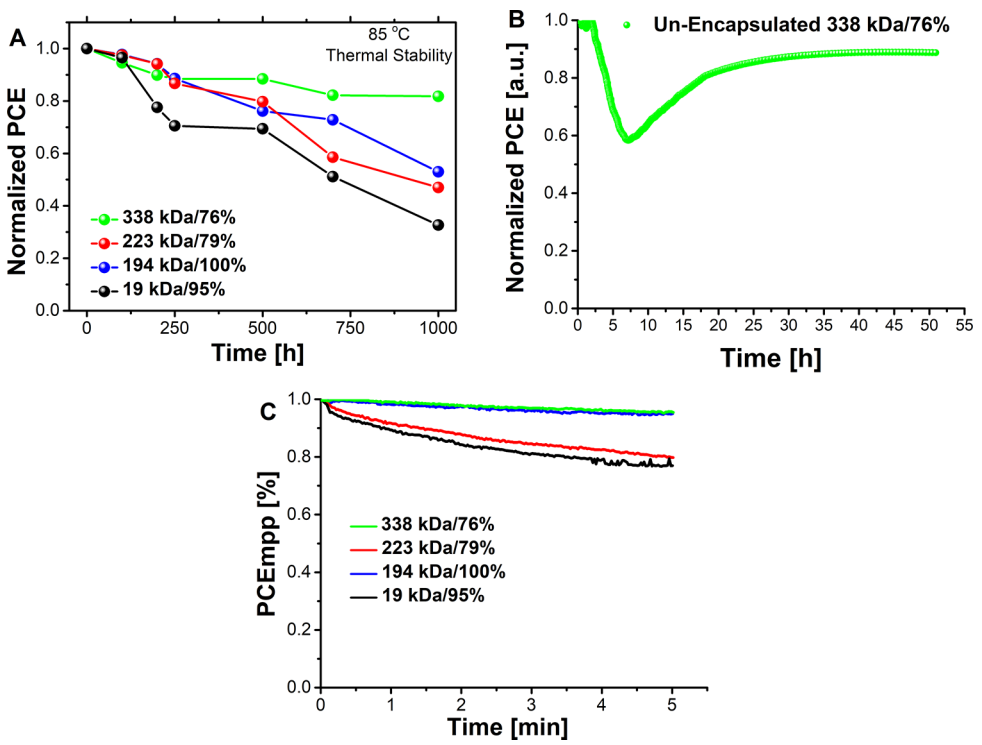

Figure 5. (A) Thermal stability of large-area (1.0 cm^2 active area) PSCs with different (MW-RR) P3HTs as HTM under continuous 85 °C thermal stress (RH: 70%). The devices were encapsulated by glass and thread seal tape. (B) Continuous light soaking of unencapsulated large-area PSCs containing the highest molecular weight (338 kDa/76%) P3HT as HTM under AM 1.5G, RH = 70% humidity, and 65 °C of the test site. (C) Maximum power point tracking (MPPT) of all MW P3HT large-area PSCs (1.0 cm^2 active area) under 1 sun (AM 1.5G) continuous illumination measured in air at RH = 70% and 65 °C of the test site.

https://doi.org/10.1021/acssuschemeng.0c09015
ACS Sustainable Chem. Eng. XXXX, XXX, XXX−XXX

intensity in a perovskite/selective layer stack is due to efficient charge extraction from the perovskite into the selective layer. We observed that P3HT with a higher MW shows a higher quenching magnitude with respect to the lower-MW P3HT. This fact confirms our previous claim concerning the improved charge extraction in correlation to a higher MW of the P3HT HTL. This element is crucial to avoid nonradiative recombination at the interface and achieve a higher V_{oc}.[83] Also, P3HTs with higher RRs show a higher quenching magnitude with respect to the lower RR counterparts. The SEM image from the surface of the bare perovskite layer is also presented in Figure 3f. The image shows good surface coverage of pinhole-free perovskite crystals with a grain size range of 200−400 nm.

Optoelectronic Characteristics of PSCs. We carried out cyclic voltammetry (CV) analyses of the PSCs with different MWs of P3HT under the dark condition and the −1.5 to 1.5 V voltage range. The Tafel plots of the CV analysis are shown in Figure 4a.

By applying a bias (dark condition), the current flowing through the device could be expressed as[27,41,70]

$$I = I_{01}\, e^{V-IR_S/2kt/q} + I_{02}\, e^{V-IR_S/kt/q} + \frac{V - IR_S}{R_{SH}} \quad (1)$$

where I_{01} and I_{02} are diode saturation currents and R_S and R_{SH} are the series and shunt resistance of the device, respectively. Owing to eq 1, the plot is divided into four bias regions: (1) <V1, dark current; (2) V1−V2, the dominant term that is related to the recombination in the depletion zone; (3) V2−V3, which is related to trap-assisted and radiative recombination; and (4) >V3, dark current that is limited by series resistance and will saturate.

In our devices, by increasing the P3HT MW, recombination in the depletion zone occurred at lower voltage ranges. This clearly shows a positive effect of the presence of high-MW HTL at the perovskite/HTL interface, enhancing the rate of hole extraction and reducing the direct recombination, which is the third term on the right-hand side of eq 1. At V2, when the bias voltage exceeded the kink point corresponding to the trap-filled limit voltage (V_{TFL}),[65,66] the current enhanced quickly, indicating that the trap states were filled. The dark JV result demonstrated that the photovoltaic improvement reached by tuning the MW of P3HT is due to the notable decrease in charge recombination. Transient photocurrent (TPC) and transient photovoltage (TPV) analyses are performed for P3HT-based PSCs. The extracted charge versus J_{sc} is measured from TPC[73,76] and plotted in Figure 4b. An evident improvement in hole extraction by tuning the MW from low to high has been demonstrated. Once more (as already evidenced for PCE measurements), the complete RR of 194 kDa was proved to be an added value to improve the photoelectrochemical properties of the HTL. In addition, from TPV,[76] the recombination time was evaluated (Figure 4c). It shows longer recombination times with increasing MWs, reducing the amount of recombination centers, confirmed also by dark JV.

Stability of PSCs. To evaluate the thermal stability of the devices, we performed thermal stress tests at 85 °C monitoring the PCE of the devices during that time and comparing the relative decrease in performance, as shown in Figure 5a. The test was performed out of glovebox and up to 1000 h with sealed devices and for all different P3HTs. The thermal stability of the devices evidences a direct relation with an increase of MW and an increase of RR: 338 kDa/76%; the MW retained more than 80% of its initial efficiency after 1000 h of thermal stress at 85 °C with an extracted T80 lifetime of 1108 h (please see Figure S9). On the other hand, a higher RR had a positive effect on the stability too: indeed, by comparing 194 kDa/100% and 223 kDa/79% P3HTs, the 194 kDa/100% one shows a slightly higher thermal stability. Along with thermal stability, it is important to evaluate the stability under operating conditions of these PSCs; therefore, light stability tests were carried out on the P3HT-based devices to evaluate the effect of molecular weight of the polymer. Maximum power point tracking (MPPT) of all P3HT large-area PSCs under 1 sun (AM 1.5G) continuous illumination measured in air at 70% relative humidity (RH) is presented in Figure 5c, and the MPP (maximum power point) stability of P3HT 100% RR is comparable to the one of the polymer with the highest MW. The highest MW P3HT (338 kDa) retains over 85% of its initial efficiency after more than 3000 min under continuous light soaking (AM 1.5G), as shown in Figure 5b. It is worth noting, however, that there is an initial drop in efficiency, as for the other samples, which is then recovered. Often, the efficiency of PSCs when exposed to light soaking initially shows a fast, exponential decay phase; yet, these losses are generally recoverable at dark conditions.[84] Nie et al. proposed the physical origin of this phenomenon as the formation of spatially localized and deep charge states (or small polarons) within the band gap of the perovskite.[85] These charged states coexist with the conventional photogenerated free carriers, dominating the photocurrent, resulting in photodegradation of the devices. However, differently from PSCs containing molecular HTMs (e.g., spiro-OMeTAD), devices employing polymeric HTMs usually show a recovery of efficiency after the fast initial decay, during a continuous MPP tracking at light soaking conditions.[27,30,46] In particular, Nia et al. demonstrated that the enhancement of polaron delocalization on the polymeric chains through the combined effect of doping strategy and MW tuning can markedly improve the efficiency and stability of the PSCs using polymeric HTMs.[30] Accordingly, the efficiency recovery of the polymer-based PSCs during light soaking analysis might be attributed to light-induced delocalization of the polarons in the polymeric HTM thin film, which can positively neutralize the photogenerated small polarons of the perovskite layer through an interfacial reaction route.

The final state probably achieved a better contact of the HTM with the perovskite and a better charge extraction ability.[86] A picture of the unencapsulated device is presented in Figure S10. The morphology and the grain size of the perovskite-layer microscopy (SEM) imaging before (fresh) and after thermal stress are presented in Figure 6a−f. The fresh P3HT surface is very smooth and has a mirrorlike appearance, and no pinholes into the perovskite or polymer surface can be observed with the various MW P3HT layers, as investigated by top-view and cross-sectional scanning electron microscopies.

The analysis of a thermally stressed low-MW P3HT (19 kDa/95%) film over perovskite, Figure 6b, evidences the formation of holes in the film (as also witnessed by SEM cross-section images in Figure 6e). Conversely, the highest MW polymer (338 kDa/76%) film has a lower density of pinholes after thermal stress (Figure 6d,f).

This also corresponds to a reduced gold diffusion through the HTL toward the perovskite or TiO_2 layer and, therefore,

https://doi.org/10.1021/acssuschemeng.0c09015
ACS Sustainable Chem. Eng. XXXX, XXX, XXX−XXX

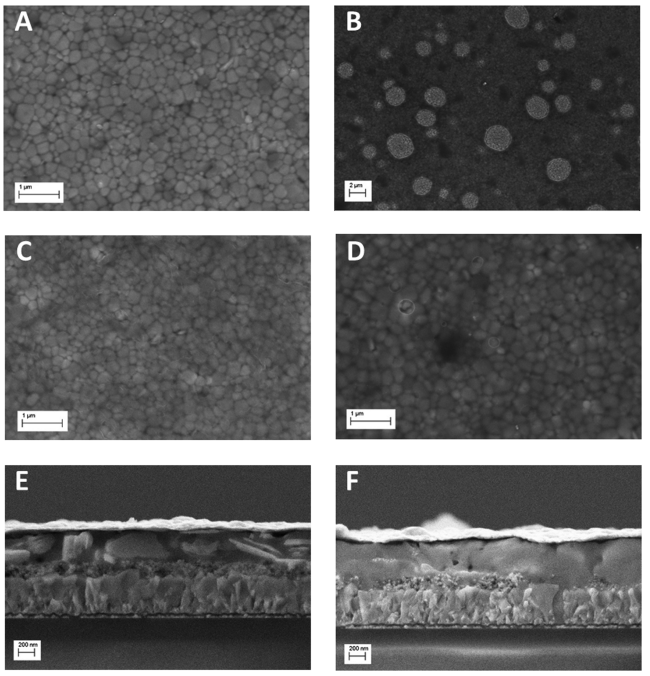

Figure 6. (A) Surface SEM of fresh 19 kDa/95%. (B) Surface SEM of stressed 19 kDa/95%. (C) Surface SEM of fresh 338 kDa/76%. (D) Surface SEM of stressed 338 kDa/76%. (E) Cross-section SEM of stressed 19 kDa/95%. (F) Cross-section SEM of stressed 338 kDa/76%.

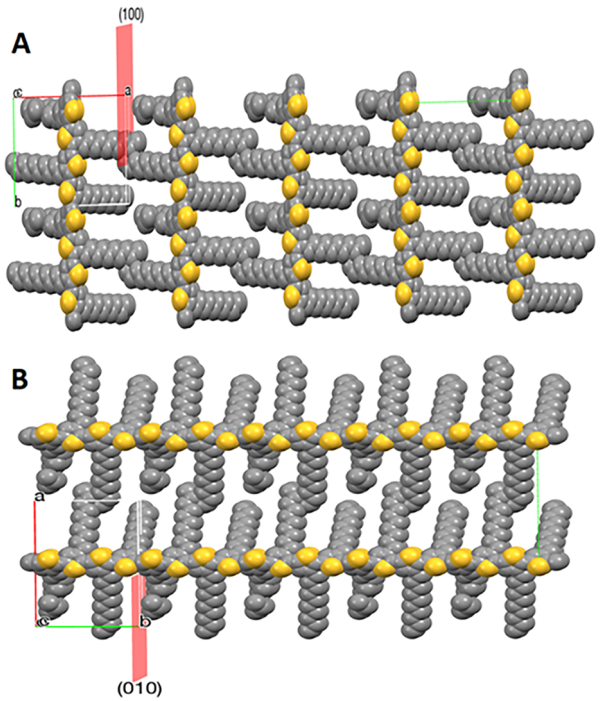

Figure 7. Lattice orientational expansion of P3HT across (A) (100) and (B) (010) crystallographic planes. The figures are produced through packing/slicing of the P3HT single-crystal information file[87] using Mercury 3.8 software.

lower shunting in the solar cell. As previously shown in the literature, increasing the MW of a polymer can reduce chain dynamics, allowing for higher thermal robustness and higher glass-transition temperatures.[81] This explanation justifies the lower degree of morphological change occurring in the high-MW P3HT layer after the thermal stress at 85 °C. At the same time, a higher chain density may also result in improved impermeability to external agents, namely, water and oxygen, which could account for additional stability in a damp heat test (i.e., 85% humidity at 85 °C).

Computational Study on the Polymer Crystal Organization. Lattice orientational growth of the polymeric layer during spin-casting can directly affect the stability and conductivity performances of the HTL. As aforementioned from GIWAXS analysis results, lower MWs show a preferential stacking along the (100) plane, while higher MWs represent more preferential stacking along the (010) plane of the P3HT crystalline lattice. To gain a better understanding of the lattice orientational growth of these two planes, we produced the packing/slicing of the P3HT (space-filled molecular style) along the (100) and (010) planes using a reported single-crystal information file[87] and Mercury software (Figure 7). As presented in the figure, the main difference in the stability and mobility performance of the P3HT with high and low MWs (lower and higher RR) can be attributed to the steric hindrance of the hexyl group. The high-molecular-weight (HMW) polymeric chains prefer to grow on the (010) plane, which prepare a suitable in-plane interchain connectivity between thiophene groups and high out-of-plane steric hindrance of hexyl groups. This steric hindrance of the hydrophobic substituents led to impenetrability of the polymeric film against polar and/or ionic compounds, which can be formed inside the cell during thermal and light stresses. Furthermore, stacking of the polymeric chains along these two important planes would be relevant to the degree of polymeric RR.

Since neighboring polymer chains interact strongly via $\pi-\pi$ interaction between the thiophene rings and by van der Waals interaction between the alkyl substitutions, these interactions give rise to two-dimensional sheets (lamellae) with ordering of the polymer backbones along the π-stacking direction. Carrier mobility within a lamella is enabled by the delocalization of the carriers in the π-stacking direction.[88] Interactions between the alkyl side chains originating from neighboring lamellae can give rise to ordered stacking in the third dimension, thereby forming P3HT crystals. Indeed, P3HT polymer chains with predominantly head-to-tail ordering (RR) can be orderly stacked along the planes via self-assembly of the non-interdigitated lamellae and enhance $\pi-\pi$ stacking, leading to improved carrier mobility across the layer.[89]

However, lower-MW polymers with preferential stacking along the (100) plane have more alkyl side chains in-plane, which lead to more stacking via van der Waals interaction and more out-of-plane access to thiophene rings without any steric hindrance. This crystalline configuration of lower-MW polymers might be the main reason for their lower performance and stability compared to high-MW P3HT layers. In particular, such a preferential orientation of lower-MW polymers causes unfavorable stacking of the P3HT chains on the hexyl steric hindrance along to the charge carrier direction inside the HTM layer (opposite to the π-stacking direction) and hinders charge extraction from the perovskite active layer.

CONCLUSIONS

In this paper, the effect of both molecular weight (MW) and regioregularity (RR) of the P3HT hole-transporting layer (HTL) on the stability of perovskite solar cells is thoroughly

https://doi.org/10.1021/acssuschemeng.0c09015
ACS Sustainable Chem. Eng. XXXX, XXX, XXX−XXX

investigated. We synthesized four P3HT polymers, following different synthetic routes, to modulate both MW and RR. All of the materials showed excellent thermal stability but different crystallinity related to their RR. XRD and GIWAXS analyses were performed on P3HT films of different RRs and MWs, and the role of the structural properties was discussed. A preliminary XRD analysis assessed the perfect reproducibility of perovskite structural properties, thus enabling an accurate investigation of the P3HT layers to be carried out, excluding disturbance of the underlying films. GIWAXS analysis proved the P3HT structural evolution related to the polymeric MW, evidencing that lower MWs correspond to higher crystallinity of the HTL, in agreement with DSC data.

Relevant to the internal orientation of P3HT crystalline domains, the effect of RR on structural properties was also explored. Specifically, high RR promotes a preferential edge-on configuration (not influencing crystallinity itself) and higher RR combined with lower MWs induces a preferential edge-on configuration with the polymers oriented with the alkyl chains stacked normal to the substrate. On the contrary, lower RR combined with higher-MW P3HT films are found to be oriented in a face-on configuration, with the thiophene rings parallel to the substrate. Concerning the optoelectronic properties, no clear difference could be evidenced due to the high similarity of the chemical structure of the materials. Thus, any modification in the performance of the HTMs should be related to how the minimal structural differences affect the morphology of the deposited film. From this point of view, evidence is gained that both MW and RR are of paramount importance in controlling both the device efficiency and stability. HTLs, once implemented in complete PSCs, showed interesting results, reaching an efficiency higher than 17% and more than 1000 h of thermal stability at 85 °C in an oven (out of glovebox). A higher MW accounted in general for the better performance since it gives smooth and pinhole-free films. Indeed, the examination and comparison of two polymers having similar RR but very different MWs (19 vs 194 kDa) showed that the latter parameter is crucial to obtain a PCE improvement. On the other hand, the comparison of two polymers with similar MW but different RRs (RR 100% for 194 kDa vs 79% for 223 kDa) showed that also this latter parameter should not be neglected to improve device efficiency. It should also be pointed out that high P3HT 338 kDa/76% can be obtained at a fraction of the cost normally needed for conventional P3HTs, which is a valuable factor toward the large-scale production of PSCs.

■ ASSOCIATED CONTENT

Supporting Information

The Supporting Information is available free of charge at https://pubs.acs.org/doi/10.1021/acssuschemeng.0c09015.

Materials and methods, all polymer synthesis procedures, polymer characterizations, device preparation, and characterization (PDF)

■ AUTHOR INFORMATION

Corresponding Authors

Pierluigi Quagliotto − *Dipartimento di Chimica and NIS Interdepartmental Centre and INSTM Reference Centre, Università degli Studi di Torino, Turin 10125, Italy;* orcid.org/0000-0002-7984-6839; Phone: +39-011-6707593; Email: pierluigi.quagliotto@unito.it

Aldo Di Carlo − *CHOSE (Centre for Hybrid and Organic Solar Energy), University of Rome "Tor Vergata", Rome 00133, Italy; Consiglio Nazionale delle Ricerche-Istituto di Struttura della Materia (CNR-ISM), Area di Ricerca di Tor Vergata, Rome 00133, Italy;* orcid.org/0000-0001-6828-2380; Phone: +39-06-72597456; Email: aldo.dicarlo@uniroma2.it

Authors

Narges Yaghoobi Nia − *CHOSE (Centre for Hybrid and Organic Solar Energy), University of Rome "Tor Vergata", Rome 00133, Italy;* orcid.org/0000-0001-6851-5156

Matteo Bonomo − *Dipartimento di Chimica and NIS Interdepartmental Centre and INSTM Reference Centre, Università degli Studi di Torino, Turin 10125, Italy;* orcid.org/0000-0002-1944-2664

Mahmoud Zendehdel − *CHOSE (Centre for Hybrid and Organic Solar Energy), University of Rome "Tor Vergata", Rome 00133, Italy; Kimia Solar Research Institute (K.S.R.I.), Kimia Solar Company, Kashan 87137-45868, Iran*

Enrico Lamanna − *CHOSE (Centre for Hybrid and Organic Solar Energy), University of Rome "Tor Vergata", Rome 00133, Italy*

Mohamed M. H. Desoky − *Dipartimento di Chimica and NIS Interdepartmental Centre and INSTM Reference Centre, Università degli Studi di Torino, Turin 10125, Italy*

Barbara Paci − *Consiglio Nazionale delle Ricerche-Istituto di Struttura della Materia (CNR-ISM), Area di Ricerca di Tor Vergata, Rome 00133, Italy*

Francesca Zurlo − *Department of Chemical Science and Technologies, University of Rome Tor Vergata, Rome 00133, Italy*

Amanda Generosi − *Consiglio Nazionale delle Ricerche-Istituto di Struttura della Materia (CNR-ISM), Area di Ricerca di Tor Vergata, Rome 00133, Italy;* orcid.org/0000-0001-5940-389X

Claudia Barolo − *Dipartimento di Chimica and NIS Interdepartmental Centre and INSTM Reference Centre, Università degli Studi di Torino, Turin 10125, Italy; ICxT Interdepartmental Centre, Università degli Studi di Torino, Turin 10153, Italy;* orcid.org/0000-0003-0627-2579

Guido Viscardi − *Dipartimento di Chimica and NIS Interdepartmental Centre and INSTM Reference Centre, Università degli Studi di Torino, Turin 10125, Italy*

Complete contact information is available at: https://pubs.acs.org/10.1021/acssuschemeng.0c09015

Author Contributions

The manuscript was written through contributions of all authors.

Notes

The authors declare no competing financial interest.

■ ACKNOWLEDGMENTS

This work was supported by the Italian Ministry of Economic Development in the framework of the Operating Agreement with ENEA for Research on the Electric System. The authors are grateful to Marco Guaragno (CNR-ISM) for his technical support with X-ray experiments.

REFERENCES

(1) Kojima, A.; Teshima, K.; Shirai, Y.; Miyasaka, T. Organometal Halide Perovskites as Visible-Light Sensitizers for Photovoltaic Cells. *J. Am. Chem. Soc.* **2009**, *131*, 6050−6051.

(2) Lee, M. M.; Teuscher, J.; Miyasaka, T.; Murakami, T. N.; Snaith, H. J. Efficient Hybrid Solar Cells Based on Meso-Superstructured Organometal Halide Perovskites. *Science* **2012**, *338*, 643−647.

(3) NREL Research Cells Efficiency Chart, 2020. http://www.nrel.gov/ncpv/images/efficiency_chart.jpg (accessed Mar 5, 2020).

(4) Zendehdel, M.; Yaghoobi Nia, N.; Yaghoubinia, M. Emerging Thin Film Solar Panels. In *Reliability and Ecological Aspects of Photovoltaic Modules*; IntechOpen, 2020.

(5) Yaghoobi Nia, N.; Saranin, D.; Palma, A. L.; Di Carlo, A. Perovskite Solar Cells. *Sol. Cells Light Manage.* **2020**, 163−228.

(6) Yaghoobi Nia, N.; Giordano, F.; Zendehdel, M.; Cinà, L.; Palma, A. L.; Medaglia, P. G.; Zakeeruddin, S. M.; Grätzel, M.; Di Carlo, A. Solution-Based Heteroepitaxial Growth of Stable Mixed Cation/Anion Hybrid Perovskite Thin Film under Ambient Condition via a Scalable Crystal Engineering Approach. *Nano Energy* **2020**, *69*, No. 104441.

(7) Leijtens, T.; Eperon, G. E.; Noel, N. K.; Habisreutinger, S. N.; Petrozza, A.; Snaith, H. J. Stability of Metal Halide Perovskite Solar Cells. *Adv. Energy Mater.* **2015**, *5*, No. 1500963.

(8) Niu, G.; Guo, X.; Wang, L. Review of Recent Progress in Chemical Stability of Perovskite Solar Cells. *J. Mater. Chem. A* **2015**, *3*, 8970−8980.

(9) Boyd, C. C.; Cheacharoen, R.; Leijtens, T.; McGehee, M. D. Understanding Degradation Mechanisms and Improving Stability of Perovskite Photovoltaics. *Chem. Rev.* **2019**, *119*, 3418−3451.

(10) Asghar, M. I.; Zhang, J.; Wang, H.; Lund, P. D. Device Stability of Perovskite Solar Cells − A Review. *Renewable Sustainable Energy Rev.* **2017**, *77*, 131−146.

(11) Valero, S.; Collavini, S.; Völker, S. F.; Saliba, M.; Tress, W. R.; Zakeeruddin, S. M.; Grätzel, M.; Delgado, J. L. Dopant-Free Hole-Transporting Polymers for Efficient and Stable Perovskite Solar Cells. *Macromolecules* **2019**, *52*, 2243−2254.

(12) Tavakoli, M. M.; Saliba, M.; Yadav, P.; Holzhey, P.; Hagfeldt, A.; Zakeeruddin, S. M.; Grätzel, M. Synergistic Crystal and Interface Engineering for Efficient and Stable Perovskite Photovoltaics. *Adv. Energy Mater.* **2019**, *9*, No. 1802646.

(13) Meng, L.; You, J.; Yang, Y. Addressing the Stability Issue of Perovskite Solar Cells for Commercial Applications. *Nat. Commun.* **2018**, *9*, No. 5265.

(14) Bai, Y.; Lin, Y.; Ren, L.; Shi, X.; Strounina, E.; Deng, Y.; Wang, Q.; Fang, Y.; Zheng, X.; Lin, Y.; Chen, Z. G.; Du, Y.; Wang, L.; Huang, J. Oligomeric Silica-Wrapped Perovskites Enable Synchronous Defect Passivation and Grain Stabilization for Efficient and Stable Perovskite Photovoltaics. *ACS Energy Lett.* **2019**, *4*, 1231−1240.

(15) Noh, J. H.; Im, S. H.; Heo, J. H.; Mandal, T. N.; Seok, S. I. Chemical Management for Colorful, Efficient, and Stable Inorganic-Organic Hybrid Nanostructured Solar Cells. *Nano Lett.* **2013**, *13*, 1764−1769.

(16) Conings, B.; Drijkoningen, J.; Gauquelin, N.; Babayigit, A.; D'Haen, J.; D'Olieslaeger, L.; Ethirajan, A.; Verbeeck, J.; Manca, J.; Mosconi, E.; De Angelis, F.; Boyen, H. G. Intrinsic Thermal Instability of Methylammonium Lead Trihalide Perovskite. *Adv. Energy Mater.* **2015**, *5*, No. 1500477.

(17) Saliba, M.; Matsui, T.; Seo, J.-Y.; Domanski, K.; Correa-Baena, J.-P.; Nazeeruddin, M. K.; Zakeeruddin, S. M.; Tress, W.; Abate, A.; Hagfeldt, A.; Gratzel, M. Cesium-Containing Triple Cation Perovskite Solar Cells: Improved Stability, Reproducibility and High Efficiency. *Energy Environ. Sci.* **2016**, *9*, 1989−1997.

(18) Ling, X.; Yuan, J.; Zhang, X.; Qian, Y.; Zakeeruddin, S. M.; Larson, B. W.; Zhao, Q.; Shi, J.; Yang, J.; Ji, K.; Zhang, Y.; Wang, Y.; Zhang, C.; Duhm, S.; Luther, J. M.; Grätzel, M.; Ma, W. Guanidinium-Assisted Surface Matrix Engineering for Highly Efficient Perovskite Quantum Dot Photovoltaics. *Adv. Mater.* **2020**, *32*, No. 2001906.

(19) Jiang, Q.; Zhao, Y.; Zhang, X.; Yang, X.; Chen, Y.; Chu, Z.; Ye, Q.; Li, X.; Yin, Z.; You, J. Surface Passivation of Perovskite Film for Efficient Solar Cells. *Nat. Photonics* **2019**, *13*, 460−466.

(20) Yang, W. S.; Park, B. W.; Jung, E. H.; Jeon, N. J.; Kim, Y. C.; Lee, D. U.; Shin, S. S.; Seo, J.; Kim, E. K.; Noh, J. H.; Seok, S. Il. Iodide Management in Formamidinium-Lead-Halide-Based Perovskite Layers for Efficient Solar Cells. *Science* **2017**, *356*, 1376−1379.

(21) Zhao, X.; Kim, H. S.; Seo, J. Y.; Park, N.-G. Effect of Selective Contacts on the Thermal Stability of Perovskite Solar Cells. *ACS Appl. Mater. Interfaces* **2017**, *9*, 7148−7153.

(22) Jena, A. K.; Numata, Y.; Ikegami, M.; Miyasaka, T. Role of Spiro-OMeTAD in Performance Deterioration of Perovskite Solar Cells at High Temperature and Reuse of the Perovskite Films to Avoid Pb-Waste. *J. Mater. Chem. A* **2018**, *6*, 2219−2230.

(23) Leijtens, T.; Ding, I.-K.; Giovenzana, T.; Bloking, J. T.; McGehee, M. D.; Sellinger, A. Hole Transport Materials with Low Glass Transition Temperatures and High Solubility for Application in Solid-State Dye-Sensitized Solar Cells. *ACS Nano* **2012**, *6*, 1455−1462.

(24) Fang, Y.; Wang, X.; Wang, Q.; Huang, J.; Wu, T. Impact of Annealing on Spiro-OMeTAD and Corresponding Solid-State Dye Sensitized Solar Cells. *Phys. Status Solidi A* **2014**, *211*, 2809−2816.

(25) Dixon, A. G.; Visvanathan, R.; Clark, N. A.; Stingelin, N.; Kopidakis, N.; Shaheen, S. E. Molecular Weight Dependence of Carrier Mobility and Recombination Rate in Neat P3HT Films. *J. Polym. Sci., Part B: Polym. Phys.* **2018**, *56*, 31−35.

(26) Rakstys, K.; Igci, C.; Nazeeruddin, M. K. Efficiency vs. Stability: Dopant-Free Hole Transporting Materials towards Stabilized Perovskite Solar Cells. *Chem. Sci.* **2019**, *10*, 6748−6769.

(27) Yaghoobi Nia, N.; Lamanna, E.; Zendehdel, M.; Palma, A. L.; Zurlo, F.; Castriotta, L. A.; Di Carlo, A. Doping Strategy for Efficient and Stable Triple Cation Hybrid Perovskite Solar Cells and Module Based on Poly(3-hexylthiophene) Hole Transport Layer. *Small* **2019**, No. 1904399.

(28) Ye, T.; Chen, W.; Jin, S.; Hao, S.; Zhang, X.; Liu, H.; He, D. Enhanced Efficiency of Planar Heterojunction Perovskite Solar Cells by a Light Soaking Treatment on Tris(Pentafluorophenyl)Borane-Doped Poly(Triarylamine) Solution. *ACS Appl. Mater. Interfaces* **2019**, *11*, 14004−14010.

(29) Lee, I.; Rolston, N.; Brunner, P.-L.; Dauskardt, R. H. Hole-Transport Layer Molecular Weight and Doping Effects on Perovskite Solar Cell Efficiency and Mechanical Behavior. *ACS Appl. Mater. Interfaces* **2019**, *11*, 23757−23764.

(30) Yaghoobi Nia, N.; Zendehdel, M.; Abdi-Jalebi, M.; Castriotta, L. A.; Kosasih, F. U.; Lamanna, E.; Abolhasani, M. M.; Zheng, Z.; Andaji-Garmaroudi, Z.; Asadi, K.; Divitini, G.; Ducati, C.; Friend, R. H.; Di Carlo, A. Beyond 17% Stable Perovskite Solar Module via Polaron Arrangement of Tuned Polymeric Hole Transport Layer. *Nano Energy* **2021**, *82*, No. 105685.

(31) Bonomo, M.; Taheri, B.; Bonandini, L.; Castro-Hermosa, S.; Brown, T. M.; Zanetti, M.; Menozzi, A.; Barolo, C.; Brunetti, F. Thermosetting Polyurethane Resins as Low-Cost, Easily Scalable, and Effective Oxygen and Moisture Barriers for Perovskite Solar Cells. *ACS Appl. Mater. Interfaces* **2020**, *12*, 54862−54875.

(32) Liu, J.; Wu, Y.; Qin, C.; Yang, X.; Yasuda, T.; Islam, A.; Zhang, K.; Peng, W.; Chen, W.; Han, L. A Dopant-Free Hole-Transporting Material for Efficient and Stable Perovskite Solar Cells. *Energy Environ. Sci.* **2014**, *7*, 2963−2967.

(33) Huang, C.; Fu, W.; Li, C. Z.; Zhang, Z.; Qiu, W.; Shi, M.; Heremans, P.; Jen, A. K. Y.; Chen, H. Dopant-Free Hole-Transporting Material with a C3h Symmetrical Truxene Core for Highly Efficient Perovskite Solar Cells. *J. Am. Chem. Soc.* **2016**, *138*, 2528−2531.

(34) Li, H.; Fu, K.; Hagfeldt, A.; Grätzel, M.; Mhaisalkar, S. G.; Grimsdale, A. C. A Simple 3,4-Ethylenedioxythiophene Based Hole-Transporting Material for Perovskite Solar Cells. *Angew. Chem., Int. Ed.* **2014**, *53*, 4085−4088.

(35) Choi, K.; Lee, J.; Kim, H. I.; Park, C. W.; Kim, G. W.; Choi, H.; Park, S.; Park, S. A.; Park, T. Thermally Stable, Planar Hybrid

https://doi.org/10.1021/acssuschemeng.0c09015
ACS Sustainable Chem. Eng. XXXX, XXX, XXX−XXX

Perovskite Solar Cells with High Efficiency. *Energy Environ. Sci.* **2018**, *11*, 3238−3247.
(36) Wang, Y.-K.; Yuan, Z.-C.; Shi, G.-Z.; Li, Y.-X.; Li, Q.; Hui, F.; Sun, B.-Q.; Jiang, Z.-Q.; Liao, L.-S. Dopant-Free Spiro-Triphenylamine/Fluorene as Hole-Transporting Material for Perovskite Solar Cells with Enhanced Efficiency and Stability. *Adv. Funct. Mater.* **2016**, *26*, 1375−1381.
(37) Yaghoobi Nia, N.; Méndez, M.; Paci, B.; Generosi, A.; Di Carlo, A.; Palomares, E. Analysis of The Efficiency Losses in Hybrid Perovskite/PTAA Solar Cells with Different Molecular Weight: Morphology vs Kinetics. *ACS Appl. Energy Mater.* **2020**, *3*, 6853−6859.
(38) Ma, W.; Yang, C.; Gong, X.; Lee, K.; Heeger, A. J. Thermally Stable, Efficient Polymer Solar Cells with Nanoscale Control of the Interpenetrating Network Morphology. *Adv. Funct. Mater.* **2005**, *15*, 1617−1622.
(39) Mardi, S.; Pea, M.; Notargiacomo, A.; Nia, N. Y.; Di Carlo, A.; Reale, A. The Molecularweight Dependence of Thermoelectric Properties of Poly (3-Hexylthiophene). *Materials* **2020**, *13*, 1404.
(40) Brabec, C. J.; Durrant, J. R. Solution-Processed Organic Solar Cells. *MRS Bull.* **2011**, *33*, 670−675.
(41) Rodrigues, A.; Castro, M. C. R.; Farinha, A. S. F.; Oliveira, M.; Tomé, J. P. C.; Machado, A. V.; Raposo, M. M. M.; Hilliou, L.; Bernardo, G. Thermal Stability of P3HT and P3HT:PCBM Blends in the Molten State. *Polym. Test.* **2013**, *32*, 1192−1201.
(42) Jacoby, M. Low-Cost Polymer Works Well in Perovskite Solar Cells. *Chem. Eng. News* **2019**, *97*, No. 11.
(43) Janasz, L.; Chlebosz, D.; Gradzka, M.; Zajaczkowski, W.; Marszalek, T.; Müllen, K.; Ulanski, J.; Kiersnowski, A.; Pisula, W. Improved Charge Carrier Transport in Ultrathin Poly(3-Hexylthiophene) Films via Solution Aggregation. *J. Mater. Chem. C* **2016**, *4*, 11488−11498.
(44) Hrostea, L.; Girtan, M.; Mallet, R.; Leontie, L. Optical and Morphological Properties of P3HT and P3HT: PCBM Thin Films Used in Photovoltaic Applications. *IOP Conf. Ser.: Mater. Sci. Eng.* **2018**, *374*, No. 012015.
(45) Wang, X.; Ederth, T.; Inganäs, O. In Situ Wilhelmy Balance Surface Energy Determination of Poly(3-Hexylthiophene) and Poly(3,4-Ethylenedioxythiophene) during Electrochemical Doping-Dedoping. *Langmuir* **2006**, *22*, 9287−9294.
(46) Jung, E. H.; Jeon, N. J.; Park, E. Y.; Moon, C. S.; Shin, T. J.; Yang, T. Y.; Noh, J. H.; Seo, J. Efficient, Stable and Scalable Perovskite Solar Cells Using Poly(3-Hexylthiophene). *Nature* **2019**, *567*, 511−515.
(47) Yaghoobi Nia, N.; Matteocci, F.; Cina, L.; Di Carlo, A. High-Efficiency Perovskite Solar Cell Based on Poly(3-Hexylthiophene): Influence of Molecular Weight and Mesoscopic Scaffold Layer. *ChemSusChem* **2017**, *10*, 3854−3860.
(48) Yaghoobi Nia, N.; Méndez, M.; Di Carlo, A.; Palomares, E. Energetic Disorder in Perovskite/Polymer Solar Cells and Its Relationship with the Interfacial Carrier Losses. *Philos. Trans. R. Soc., A* **2019**, *377*, No. 20180315.
(49) Zhu, Z.; Zhao, D.; Chueh, C. C.; Shi, X.; Li, Z.; Jen, A. K. Y. Highly Efficient and Stable Perovskite Solar Cells Enabled by All-Crosslinked Charge-Transporting Layers. *Joule* **2018**, *2*, 168−183.
(50) Blanchard, L.-P.; Hesse, J.; Malhotra, S. L. Effect of Molecular Weight on Glass Transition by Differential Scanning Calorimetry. *Can. J. Chem.* **1974**, *52*, 3170−3175.
(51) Derue, L.; Dautel, O.; Tournebize, A.; Drees, M.; Pan, H.; Berthumeyrie, S.; Pavageau, B.; Cloutet, E.; Chambon, S.; Hirsch, L.; Rivaton, A.; Hudhomme, P.; Facchetti, A.; Wantz, G. Thermal Stabilisation of Polymer-Fullerene Bulk Heterojunction Morphology for Efficient Photovoltaic Solar Cells. *Adv. Mater.* **2014**, *26*, 5831−5838.
(52) Griffini, G.; Douglas, J. D.; Piliego, C.; Holcombe, T. W.; Turri, S.; Fréchet, J. M. J.; Mynar, J. L. Long-Term Thermal Stability of High-Efficiency Polymer Solar Cells Based on Photocrosslinkable Donor-Acceptor Conjugated Polymers. *Adv. Mater.* **2011**, *23*, 1660−1664.
(53) Kang, H.; Uddin, M. A.; Lee, C.; Kim, K. H.; Nguyen, T. L.; Lee, W.; Li, Y.; Wang, C.; Woo, H. Y.; Kim, B. J. Determining the Role of Polymer Molecular Weight for High-Performance All-Polymer Solar Cells: Its Effect on Polymer Aggregation and Phase Separation. *J. Am. Chem. Soc.* **2015**, *137*, 2359−2365.
(54) Wang, T. L.; Hsieh, T. H. Effect of Polyol Structure and Molecular Weight on the Thermal Stability of Segmented Poly-(Urethaneureas). *Polym. Degrad. Stab.* **1997**, *55*, 95−102.
(55) Yang, X.; Zhong, Z.; Huang, Y. The Effect of PEG Molecular Weights on the Thermal Stability and Dissolution Behaviors of Griseofulvin-PEG Crystalline Inclusion Complexes. *Int. J. Pharm.* **2016**, *508*, 51−60.
(56) Sánchez-Soto, P. J.; Ginés, J. M.; Arias, M. J.; Novák, C.; Ruiz-Conde, A. Effect of Molecular Mass on the Melting Temperature, Enthalpy and Entropy of Hydroxy-Terminated PEO. *J. Therm. Anal. Calorim.* **2002**, *67*, 189−197.
(57) Buckley, C. P.; Kovacs, A. J. Melting Behaviour of Low Molecular Weight Poly(Ethylene-Oxide) Fractions. In *Polymere Aspekte*; Steinkopff: Darmstadt, 2007; Vol. *254*, pp 44−52.
(58) Huang, Y. C.; Liu, W. S.; Tsao, C. S.; Wang, L. Mechanistic Insights into the Effect of Polymer Regioregularity on the Thermal Stability of Polymer Solar Cells. *ACS Appl. Mater. Interfaces* **2019**, *11*, 40310−40319.
(59) Kim, Y.; Cook, S.; Tuladhar, S. M.; Choulis, S. A.; Nelson, J.; Durrant, J. R.; Bradley, D. D. C.; Giles, M.; McCulloch, I.; Ha, C. S.; Ree, M. A Strong Regioregularity Effect in Self-Organizing Conjugated Polymer Films and High-Efficiency Polythiophene:Fullerene Solar Cells. *Nat. Mater.* **2006**, *5*, 197−203.
(60) Sivula, K.; Luscombe, C. K.; Thompson, B. C.; Fréchet, J. M. J. Enhancing the Thermal Stability of Polythiophene:Fullerene Solar Cells by Decreasing Effective Polymer Regioregularity. *J. Am. Chem. Soc.* **2006**, *128*, 13988−13989.
(61) Chuang, S. Y.; Chen, H. L.; Lee, W. H.; Huang, Y. C.; Su, W. F.; Jen, W. M.; Chen, C. W. Regioregularity Effects in the Chain Orientation and Optical Anisotropy of Composite Polymer/Fullerene Films for High-Efficiency, Large-Area Organic Solar Cells. *J. Mater. Chem.* **2009**, *19*, 5554−5560.
(62) Quagliotto, P.; Fin, A. Advances in Synthetic Methods for the Preparation of Poly(3- Hexylthiophene) (P3HT). *Lett. Org. Chem.* **2018**, *15*, 991−1006.
(63) Shi, X.; Sui, A.; Wang, Y.; Li, Y.; Geng, Y.; Wang, F. Controlled Synthesis of High Molecular Weight Poly(3-Hexylthiophene)s via Kumada Catalyst Transfer Polycondensation with Ni(IPr)(Acac)2as the Catalyst. *Chem. Commun.* **2015**, *51*, 2138−2140.
(64) Sugimoto, R. I.; Yoshino, K.; Hayashi, S. Preparation and Properties of Conducting Heterocyclic Polymer Films by Chemical Method. *Jpn. J. Appl. Phys.* **1984**, *23*, L899−L900.
(65) Pratt, C. M.; Foot, P. J. S.; Davis, R. Effects of Cocl2 and Other Additives on the Oxidative Chemical Synthesis and Properties of Poly(3-Hexylthiophene). *Polym. Polym. Compos.* **2016**, *24*, 185−190.
(66) Shi, X.; Sui, A.; Wang, Y.; Li, Y.; Geng, Y.; Wang, F. Controlled Synthesis of High Molecular Weight Poly(3-Hexylthiophene)s via Kumada Catalyst Transfer Polycondensation with Ni(IPr)(Acac)2 as the Catalyst. *Chem. Commun.* **2015**, *51*, 2138−2140.
(67) Kline, R. J.; McGehee, M. D.; Kadnikova, E. N.; Liu, J.; Fréchet, J. M. J.; Toney, M. F. Dependence of Regioregular Poly(3-Hexylthiophene) Film Morphology and Field-Effect Mobility on Molecular Weight. *Macromolecules* **2005**, *38*, 3312−3319.
(68) Dang, M. T.; Hirsch, L.; Wantz, G.; Wuest, J. D. Controlling the Morphology and Performance of Bulk Heterojunctions in Solar Cells. Lessons Learned from the Benchmark Poly(3-Hexylthiophene): [6,6]-Phenyl- C61-Butyric Acid Methyl Ester System. *Chem. Rev.* **2013**, 3734−3765.
(69) Osaka, M.; Benten, H.; Lee, L. T.; Ohkita, H.; Ito, S. Development of Highly Conductive Nanodomains in Poly(3-Hexylthiophene) Films Studied by Conductive Atomic Force Microscopy. *Polymer* **2013**, *54*, 3443−3447.
(70) Niu, G.; Li, W.; Meng, F.; Wang, L.; Dong, H.; Qiu, Y. Study on the Stability of CH3NH3PbI3 Films and the Effect of Post-

https://doi.org/10.1021/acssuschemeng.0c09015
ACS Sustainable Chem. Eng. XXXX, XXX, XXX−XXX

Modification by Aluminum Oxide in All-Solid-State Hybrid Solar Cells. *J. Mater. Chem. A* **2014**, *2*, 705−710.
(71) Zhao, Y.; Gu, X.; Qiang, Y. Influence of Growth Time and Annealing on Rutile TiO 2 Single-Crystal Nanorod Arrays Synthesized by Hydrothermal Method in Dye-Sensitized Solar Cells. *Thin Solid Films* **2012**, *520*, 2814−2818.
(72) Yaghoobi Nia, N.; Zendehdel, M.; Cinà, L.; Matteocci, F.; Di Carlo, A. A Crystal Engineering Approach for Scalable Perovskite Solar Cells and Module Fabrication: A Full out of Glove Box Procedure. *J. Mater. Chem. A* **2018**, *6*, 659−671.
(73) Marin-Beloqui, J. M.; Lanzetta, L.; Palomares, E. Decreasing Charge Losses in Perovskite Solar Cells Through Mp-TiO 2 /MAPI Interface Engineering. *Chem. Mater.* **2016**, *28*, 207−213.
(74) Dacuña, J.; Salleo, A. Modeling Space-Charge-Limited Currents in Organic Semiconductors: Extracting Trap Density and Mobility. *Phys. Rev. B: Condens. Matter Mater. Phys.* **2011**, *84*, No. 195209.
(75) Dixon, A. G.; Visvanathan, R.; Clark, N. A.; Stingelin, N.; Kopidakis, N.; Shaheen, S. E. Molecular Weight Dependence of Carrier Mobility and Recombination Rate in Neat P3HT Films. *J. Polym. Sci., Part B: Polym. Phys.* **2018**, *56*, 31−35.
(76) Tan, H.; Che, F.; Wei, M.; Zhao, Y.; Saidaminov, M. I.; Todorović, P.; Broberg, D.; Walters, G.; Tan, F.; Zhuang, T.; Sun, B.; Liang, Z.; Yuan, H.; Fron, E.; Kim, J.; Yang, Z.; Voznyy, O.; Asta, M.; Sargent, E. H. Dipolar Cations Confer Defect Tolerance in Wide-Bandgap Metal Halide Perovskites. *Nat. Commun.* **2018**, *9*, No. 3100.
(77) Baikie, T.; Barrow, N. S.; Fang, Y.; Keenan, P. J.; Slater, P. R.; Piltz, R. O.; Gutmann, M.; Mhaisalkar, S. G.; White, T. J. A Combined Single Crystal Neutron/X-Ray Diffraction and Solid-State Nuclear Magnetic Resonance Study of the Hybrid Perovskites CH3NH3PbX3 (X = I, Br and Cl). *J. Mater. Chem. A* **2015**, *3*, 9298−9307.
(78) Woo, C. H.; Thompson, B. C.; Kim, B. J.; Toney, M. F.; Fréchet, J. M. J. The Influence of Poly(3-Hexylthiophene) Regioregularity on Fullerene-Composite Solar Cell Performance. *J. Am. Chem. Soc.* **2008**, *130*, 16324−16329.
(79) Kroon, R.; Mengistie, D. A.; Kiefer, D.; Hynynen, J.; Ryan, J. D.; Yu, L.; Müller, C. Thermoelectric Plastics: From Design to Synthesis, Processing and Structure-Property Relationships. *Chem. Soc. Rev.* **2016**, *45*, 6147−6164.
(80) Wang, S. Emerging Efficient Charge-Transport Landscape Based on Short-Range Order in Conjugated Polymers. *Synth. Met.* **2019**, 104−119.
(81) Sirringhaus, H.; Brown, P. J.; Friend, R. H.; Nielsen, M. M.; Bechgaard, K.; Langeveld-Voss, B. M. W.; Spiering, A. J. H.; Janssen, R. A. J.; Meijer, E. W.; Herwig, P.; De Leeuw, D. M. Two-Dimensional Charge Transport in Self-Organized, High-Mobility Conjugated Polymers. *Nature* **1999**, *401*, 685−688.
(82) Kim, J. S.; Kim, J. H.; Lee, W.; Yu, H.; Kim, H. J.; Song, I.; Shin, M.; Oh, J. H.; Jeong, U.; Kim, T. S.; Kim, B. J. Tuning Mechanical and Optoelectrical Properties of Poly(3-Hexylthiophene) through Systematic Regioregularity Control. *Macromolecules* **2015**, *48*, 4339−4346.
(83) Tress, W.; Marinova, N.; Inganäs, O.; Nazeeruddin, M. K.; Zakeeruddin, S. M.; Graetzel, M. Predicting the Open-Circuit Voltage of CH3NH3PbI3 Perovskite Solar Cells Using Electroluminescence and Photovoltaic Quantum Efficiency Spectra: The Role of Radiative and Non-Radiative Recombination. *Adv. Energy Mater.* **2015**, *5*, No. 1400812.
(84) Domanski, K.; Alharbi, E. A.; Hagfeldt, A.; Grätzel, M.; Tress, W. Systematic Investigation of the Impact of Operation Conditions on the Degradation Behaviour of Perovskite Solar Cells. *Nat. Energy* **2018**, *3*, 61−67.
(85) Nie, W.; Blancon, J. C.; Neukirch, A. J.; Appavoo, K.; Tsai, H.; Chhowalla, M.; Alam, M. A.; Sfeir, M. Y.; Katan, C.; Even, J.; Tretiak, S.; Crochet, J. J.; Gupta, G.; Mohite, A. D. Light-Activated Photocurrent Degradation and Self-Healing in Perovskite Solar Cells. *Nat. Commun.* **2016**, *7*, No. 11574.
(86) Irannejad, N.; Yaghoobi Nia, N.; Adhami, S.; Lamanna, E.; Rezaei, B.; Di Carlo, A. Polymer/Inorganic Hole Transport Layer for Low-Temperature-Processed Perovskite Solar Cells. *Energies* **2020**, *13*, No. 2059.
(87) Luzny, W. X-ray Diffraction and Computer Modelling Study of the Structure and Conformation of Poly(3-decylthiophene). *Acta Crystallogr., Sect. B: Struct. Sci.* **1995**, *51*, 255−260.
(88) Street, R. A.; Northrup, J. E.; Salleo, A. Transport in Polycrystalline Polymer Thin-Film Transistors. *Phys. Rev. B: Condens. Matter Mater. Phys.* **2005**, *71*, No. 165202.
(89) Xie, W.; Sun, Y. Y.; Zhang, S. B.; Northrup, J. E. Structure and Sources of Disorder in Poly(3-Hexylthiophene) Crystals Investigated by Density Functional Calculations with van Der Waals Interactions. *Phys. Rev. B: Condens. Matter Mater. Phys.* **2011**, *83*, No. 184117.

https://doi.org/10.1021/acssuschemeng.0c09015
ACS Sustainable Chem. Eng. XXXX, XXX, XXX−XXX